



T-Cell Receptor CDR3 Loop Conformations in Solution Shift the Relative $V\alpha$ - $V\beta$ Domain Distributions

Monica L. Fernández-Quintero, Nancy D. Pomarici, Johannes R. Loeffler, Clarissa A. Seidler and Klaus R. Liedl*

Center for Molecular Biosciences Innsbruck (CMBI), Department of General, Inorganic and Theoretical Chemistry, University of Innsbruck, Innsbruck, Austria

T-cell receptors are an important part in the adaptive immune system as they are responsible for detecting foreign proteins presented by the major histocompatibility complex (MHC). The affinity is predominantly determined by structure and sequence of the complementarity determining regions (CDRs), of which the CDR3 loops are responsible for peptide recognition. We present a kinetic classification of T-cell receptor CDR3 loops with different loop lengths into canonical and non-canonical solution structures. Using molecular dynamics simulations, we do not only sample available X-ray structures, but we also observe a substantially broader CDR3 loop ensemble with various distinct kinetic minima in solution. Our results strongly imply, that for given CDR3 loop sequences several canonical structures have to be considered to characterize the conformational diversity of these loops. Our suggested dominant solution structures could extend the repertoire of available canonical clusters by including kinetic minimum structures present in solution. Thus, the CDR3 loops need to be characterized as conformational ensembles in solution. Furthermore, the conformational changes of the CDR3 loops follow the paradigm of conformational selection, because the experimentally determined binding competent state is present within this ensemble of pre-existing conformations without the presence of the antigen. We also identify strong correlations between the CDR3 loops and include combined state descriptions. Additionally, we observe a strong dependency of the CDR3 loop conformations on the relative $V\alpha$ - $V\beta$ interdomain orientations, revealing that certain CDR3 loop states favor specific interface orientations.

Keywords: CDR3 loop ensembles, conformational selection, Markov-state models, relative $V\alpha/V\beta$ domain distributions, T-cell receptors, T-cell receptor structure and design

OPEN ACCESS

Edited by:

Loretta Tuosto,
Sapienza University of Rome, Italy

Reviewed by:

Erin J. Adams,
University of Chicago, United States
Charlotte Deane,
University of Oxford, United Kingdom

*Correspondence:

Klaus R. Liedl
klaus.liedl@uibk.ac.at

Specialty section:

This article was submitted to
T Cell Biology,
a section of the journal
Frontiers in Immunology

Received: 24 March 2020

Accepted: 03 June 2020

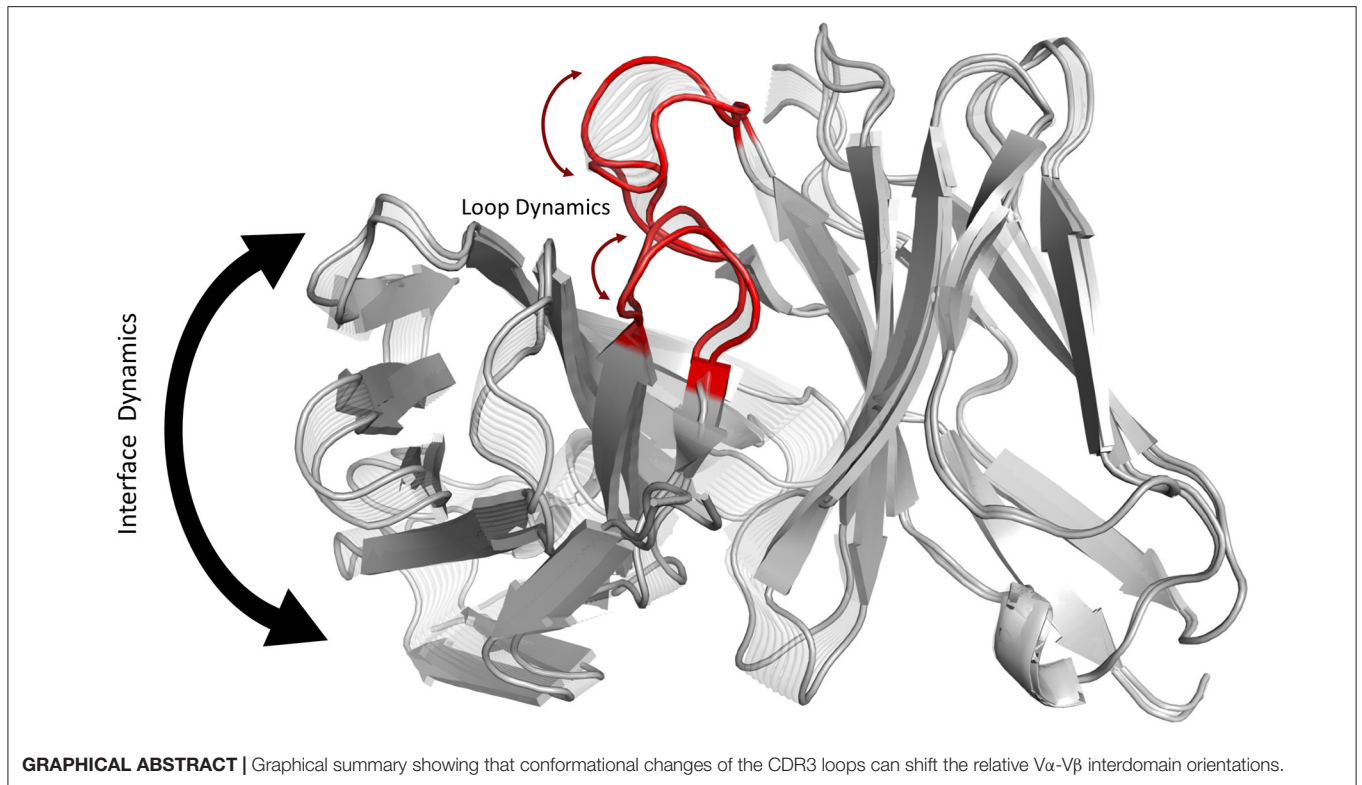
Published: 08 July 2020

Citation:

Fernández-Quintero ML, Pomarici ND, Loeffler JR, Seidler CA and Liedl KR (2020) T-Cell Receptor CDR3 Loop Conformations in Solution Shift the Relative $V\alpha$ - $V\beta$ Domain Distributions. *Front. Immunol.* 11:1440. doi: 10.3389/fimmu.2020.01440

INTRODUCTION

T-cell receptors (TCRs) play a fundamental role in the adaptive immune system and are responsible for recognizing foreign proteins (1). Depending on the type of the T-cell the TCR is expressed on, it recognizes protein fragments derived from intra- or extracellular regions, displayed by the Major Histocompatibility Complex (MHC) (2). TCRs consist of an α and a β chain analogous to the heavy and light chain in the antigen-binding fragment (Fab) of antibodies (3, 4). $V\alpha$ and $C\alpha$ can be interpreted as homologous in sequence and structure to the V_L and C_L domains in antibodies as well as $V\beta$ and $C\beta$ as equivalent to V_H and C_H (5, 6). The majority of T-cells are $\alpha\beta$ T-cells,



however, there also exist $\gamma\delta$ T-cells, which are able to recognize a broad range of antigens without the presence of major histocompatibility complex molecules. $\gamma\delta$ T-cells are an important subset of “unconventional” T lymphocytes, attacking target cells directly through their cytotoxic activity (7). TCR alpha chains are made by V and J genes, while beta chains are produced by V, D, and J genes. Sequence and structural diversity are concentrated on six hypervariable loops, also known as the complementarity determining regions (CDRs) (3, 8, 9). The CDR3 α loop reveals a diversity of length and sequence composition due to the recombination of two gene segments V and J, while the CDR3 β loop variability is increased due to the D gene (10, 11). The CDR3 loops are located in the center of the paratope and play a crucial role in the peptide recognition (12). Additionally, the CDR3 loops have been discussed to directly influence each other and to be structurally correlated (13, 14). Analogous to antibodies five of the six CDR loops adopt a limited set of main-chain conformations, so called canonical structures. Due to the high variability in sequence, length and the ability of the CDR3 loops to adopt different conformations during the V(D)J recombination, structure prediction remains challenging (15, 16). Compared to antibodies only few studies focused on characterizing and classifying TCR CDR loops into canonical classes (3, 9). Crystal structures of the same TCRs crystallized with and without pMHC (peptides presented by MHC molecules) reveal conformational changes upon binding mainly in the CDR3 loops (12, 17, 18). Compared to antibodies, TCRs reveal a higher flexibility in the CDR loops, especially in the CDR3 loops (16, 19). Analogous

to CDR loops of antibodies, TCR CDR loops follow the concept of conformational diversity, because one TCR can adopt various different conformations, which directly influence the binding properties and their functions (9). The fact, that TCRs and antibodies are derived from a similar genetic mechanism and have a nearly identical architecture and a high structural similarity, inspires an antibody-like TCR design, TCR-mimic antibodies and soluble TCRs (5, 6, 10, 11, 20–22). Apart from the CDR loops, the binding site of TCRs is also known to be affected by the relative orientation of the variable domains, $V\alpha$ and $V\beta$. The interdomain orientation influences the relative position of the CDR loops to one another and therefore changes the geometry of the antigen binding site (9, 23, 24). In addition to the variations in length and sequence of the CDRs, the modulation of the V_H and V_L interdomain orientation might not only be required means to accommodate the diverse antigenic shapes, but also a mechanism to increase the possible number of antibody paratopes (25). In this study, we investigate the conformational diversity of different TCR CDR3 loops and kinetically and thermodynamically classify the combined CDR3 loop ensembles in solution and their influence on the relative $V\alpha$ - $V\beta$ orientation. The investigated TCRs were chosen because of their strong experimental structural information and their differences in CDR3 loop lengths.

METHODS

Experimental structural information was available for all considered T-cell receptors. We deleted the co-crystallized

antigen in all complex crystal structures. The starting structures for simulations were prepared in MOE (Molecular Operating Environment, Chemical Computing Group, version 2018.01) using the Protonate3D tool (26, 27). To neutralize the charges we used the uniform background charge (28–30). Using the tleap tool of the AmberTools18 (28, 29) package, the crystal structures were soaked with cubic water boxes of TIP3P water molecules with a minimum wall distance of 10 Å to the protein (31). For all crystal structures parameters of the AMBER force field 14SB were used (32). The TCRs were carefully equilibrated using a multistep equilibration protocol (33).

Metadynamics Simulations

To enhance the sampling of the conformational space well-tempered metadynamics (34–36) simulations were performed in GROMACS (37, 38) with the PLUMED 2 implementation (39). We used metadynamics to overcome the timescale limitations of molecular dynamics simulations and to accelerate the sampling allowing the system to escape deep energy minima (35). As collective variables, we used a linear combination of sine and cosine of the ψ torsion angles of the CDR3 α and CDR3 β loops, calculated with functions MATHEVAL and COMBINE implemented in PLUMED 2 (39). As discussed previously the ψ torsion angle captures conformational transitions comprehensively (40). The decision to include the CDR3 α loop is based on the previously discussed structural correlation between the CDR3 α and CDR3 β loops (13). The simulations were performed at 300 K in an NpT ensemble. We used a Gaussian height of 10.0 kcal/mol. Gaussian deposition occurred every 1,000 steps and a biasfactor of 10 was used. One micro second of metadynamics simulations were performed for each available TCR crystal structure. The constant and variable domains of each TCR were simulated (23). The resulting trajectories were clustered in cpptraj (29, 41) by using the average linkage hierarchical clustering algorithm with a distance cut-off criterion of 1.2 Å resulting in a large number of clusters. The cluster representatives for the TCR were equilibrated and simulated for 100 ns using the AMBER18 (42) simulation package.

Molecular Dynamics Simulations

Molecular dynamics simulations were performed in an NpT ensemble using pmemd.cuda (43). Bonds involving hydrogen atoms were restrained by applying the SHAKE algorithm (44), allowing a time step of 2.0 fs. Atmospheric pressure of the system was preserved by weak coupling to an external bath using the Berendsen algorithm (45). The Langevin thermostat (46) was used to maintain the temperature during simulations at 300 K.

With the obtained trajectories we performed a time-lagged independent component analysis (tICA) using the python library PyEMMA 2 employing a lag time of 10 ns (47). Thermodynamics and kinetics were calculated with a Markov-state model (48) by using PyEMMA 2, which uses the k-means clustering algorithm (49) to define microstates and the PCCA+ clustering algorithm (50) to coarse grain the microstates to macrostates. The sampling efficiency and the reliability of the Markov-state model (e.g., defining optimal feature mappings) can be evaluated with the Chapman-Kolmogorov test (51, 52), by using the variational

approach for Markov processes (53) and by taking into account the fraction of states used, as the network states must be fully connected to calculate probabilities of transitions and the relative equilibrium probabilities. The Chapman-Kolmogorov tests for all Markov-state models presented in this study are displayed in **Figures S1–S5**. To build the Markov-state model we used the backbone torsions of the respective CDR loop, defined 150 microstates using the k-means clustering algorithm and applied a lag time of 10 ns.

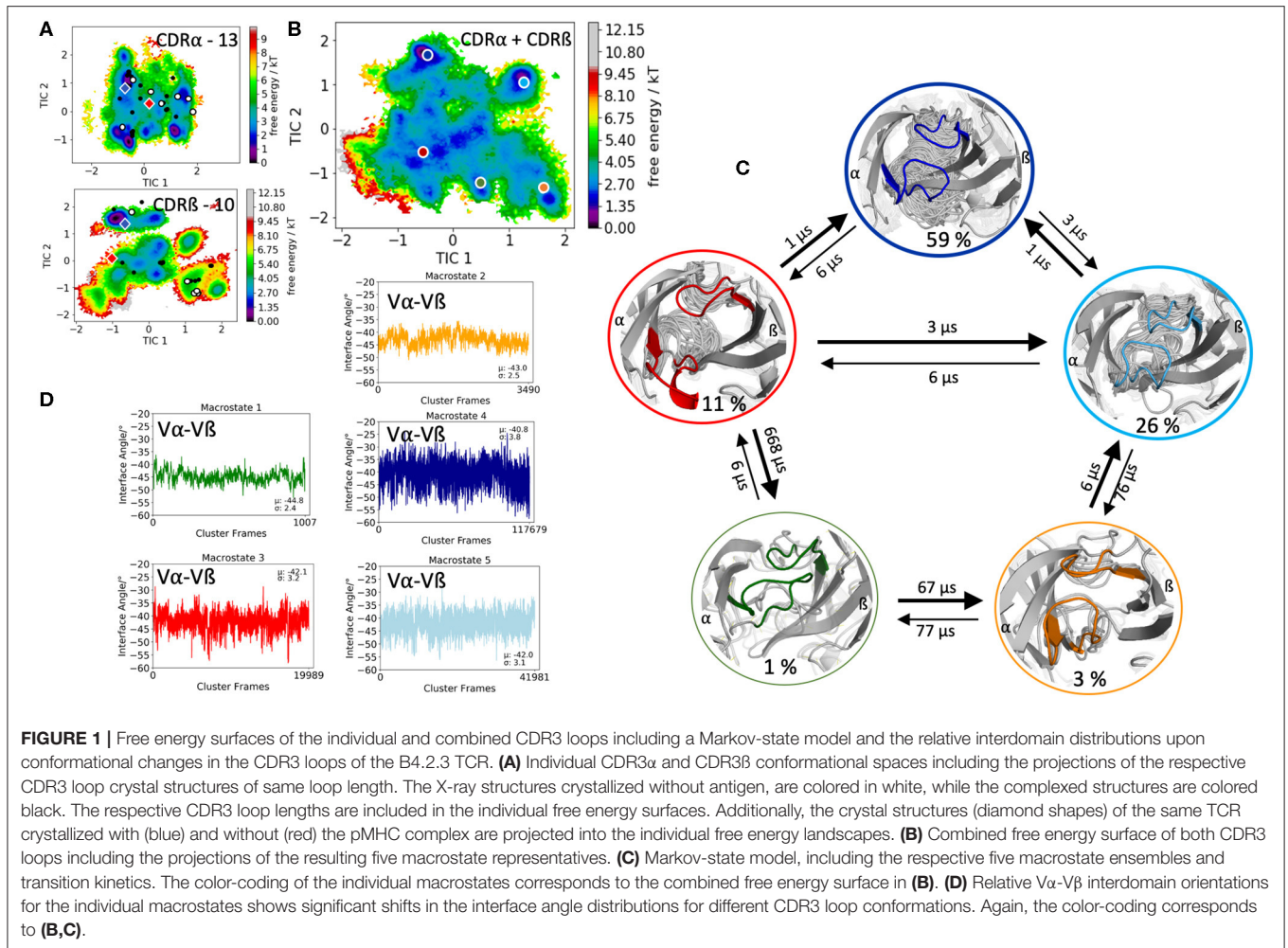
Relative V_H and V_L Orientation Calculation

For the relative V_H and V_L orientations, described in this study, we defined a torsion angle between the center of mass (COM) of the CDR loops of the light chain, the COM of the V_L domain, the COM of the V_H domain and the COM of the CDR loops of the heavy chain.

RESULTS

The first TCR studied, is the specific B4.2.3 TCR binding to the pMHC ligand P18-I10 H2-D^d. Experimental structural information with and without the pMHC complex present (PDB accession codes: 5IVX, 5IW1) indicates large structural rearrangement of the CDR3 loops upon binding. As starting structure for 1 μ s of metadynamics simulations we used the TCR structure crystallized in complex with the pMHC but simulated the TCR without the antigen. As described in the methods section, the resulting trajectory was clustered and the obtained 218 clusters, were used as starting structures for each 100 ns molecular dynamics simulations. The 21.8 μ s of trajectories were then used to construct tICA free energy landscapes for the combined and the individual CDR3 α and CDR3 β loops. The CDR3 α loop length for this specific B4.2.3 TCR is 13, while the CDR3 β loop contains 10 amino acid residues. All available TCR crystal structures of the same CDR3 loop length with a resolution <2.2 Å were used for both the CDR3 α and CDR3 β loops and projected into the respective individual free energy surfaces (**Figure 1A**). The majority of the available crystal structures are present within our obtained CDR3 α and CDR3 β ensembles in solution, indicating that also the CDR3 loops in TCRs, analogous to antibodies, can adopt various different conformations in solution and thus need to be described as conformational ensemble. As it has been shown, CDR3 α and CDR3 β loops are positively correlated and structurally influence each other, the combined conformational space of the CDR3 loops is shown in **Figure 1B** and the Markov-state model and transition times are shown in **Figure 1C**. We observe five macrostates and transition kinetics in the high microsecond timescale. **Figure 1D** displays the relative $V\alpha$ - $V\beta$ interdomain orientation of the respective CDR3 macrostate ensembles and we can clearly see a strong shift in the angle distributions upon conformational changes in the CDR3 loops.

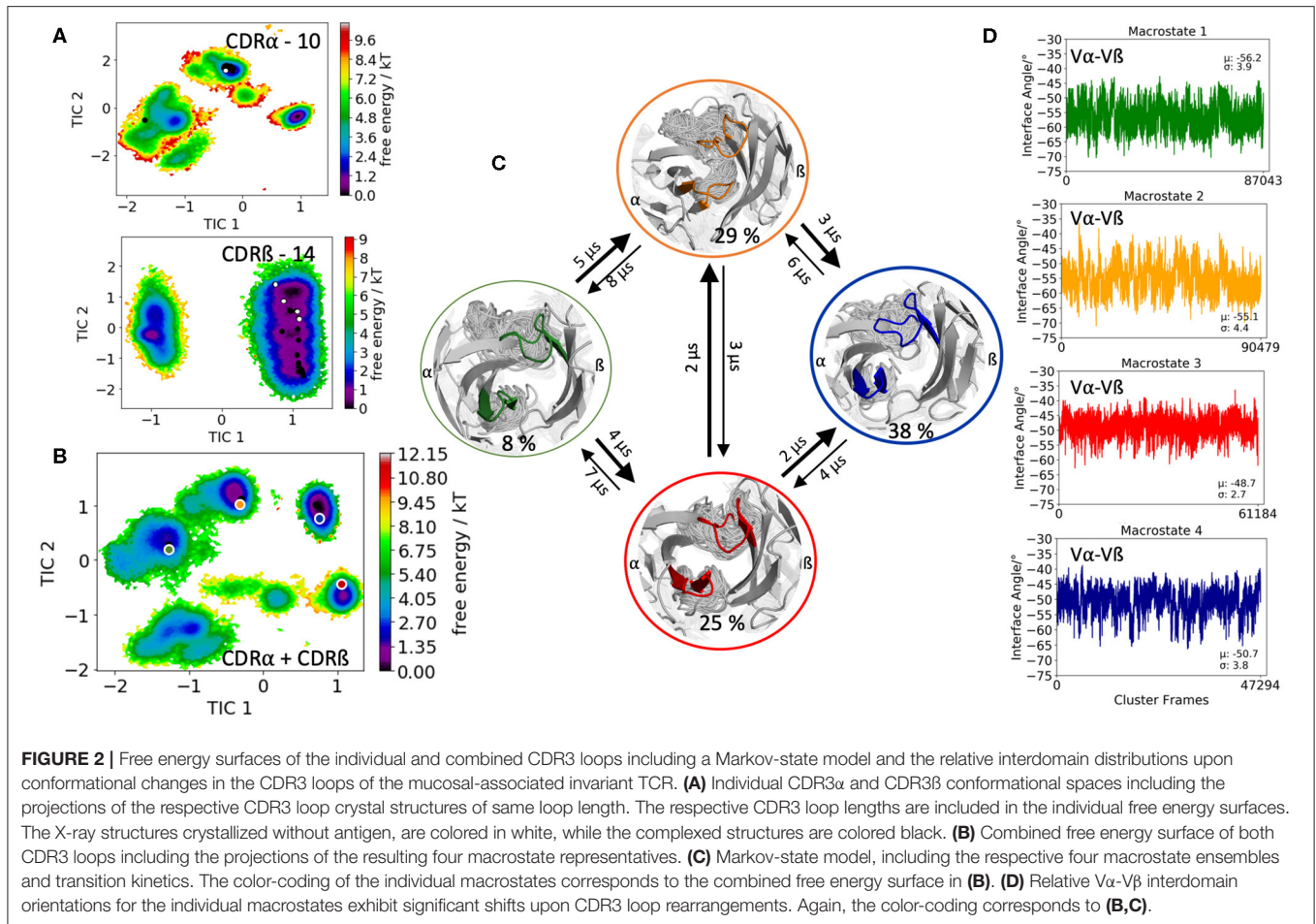
The second TCR investigated, is the receptor of the mucosal-associated invariant T cells (MAIT cells) binding to the major-histocompatibility-complex-(MHC)-class-I-related molecule MR1 and a vitamin-B-based ligand (PDB accession code: 5U2V) (54). The CDR3 α loop consists of 10 amino acid



residues, while the CDR3 β contains 14 residues. Clustering of the 1 μ s metadynamics trajectory resulted in 287 cluster representatives that were used as starting structures for each 100 ns of molecular dynamics simulations. **Figure 2A** shows the resulting conformational diversity of 28.7 μ s of trajectories of the individual CDR3 α and CDR3 β loops including the projection of the available TCR crystal structures of same length. We again clearly see that the majority of available TCR crystal structures for the CDR3 α and CDR3 β loops lie within our ensemble in solution, stressing the fact that one single static structure is not enough to capture the high flexibility of these loops. Besides sampling the majority of crystal structures, **Figure 2A** shows additional dominant solution structures, which might be included when characterizing CDR3 α and CDR3 β loop ensembles. The combined conformational space of the CDR3 α and CDR3 β loops is illustrated in **Figure 2B** and reveals four macrostates with conformational transitions in the microsecond timescale (**Figure 2C**). Again, the obtained macrostate ensembles were used to calculate the relative V α -V β interdomain distributions to identify the influence of different CDR3 loop conformations on the interface orientations. Excitingly,

we observe substantial shifts in the V α -V β interdomain distributions upon conformational changes in the CDR3 loops (**Figure 2D**).

Another TCR studied, is part of an *in silico* and structural study investigating TCR loop flexibility and the influence of crystallization conditions and crystal packing effects on the loop flexibility (19). As starting structure for our simulation we used the 003 TCR that recognizes an HIV p17 Gag-derived peptide (SLYNTVATL) presented by HLA-A*0201 with the PDB accession code 6FR4. In this case the CDR3 α loop length consists of 9 amino acids, while the CDR3 β loop is 12 residues long. The obtained 182 cluster representatives of the metadynamics simulations were used as starting structures for each 100 ns molecular dynamics simulations to reconstruct the free energy surfaces of the individual and the combined CDR3 α and CDR3 β conformational spaces (**Figures 3A,B**). The results in **Figure 3A** clearly show the extraordinarily high flexibility of the individual CDR3 loops, in particular the CDR3 β loop, because the majority of available TCR crystal structures with the CDR3 α loop length of 9 residues and the CDR3 β loop consisting of 12 residues are present within our obtained ensemble in solution. For the combined CDR3 loop states in **Figure 3C** we observe transition

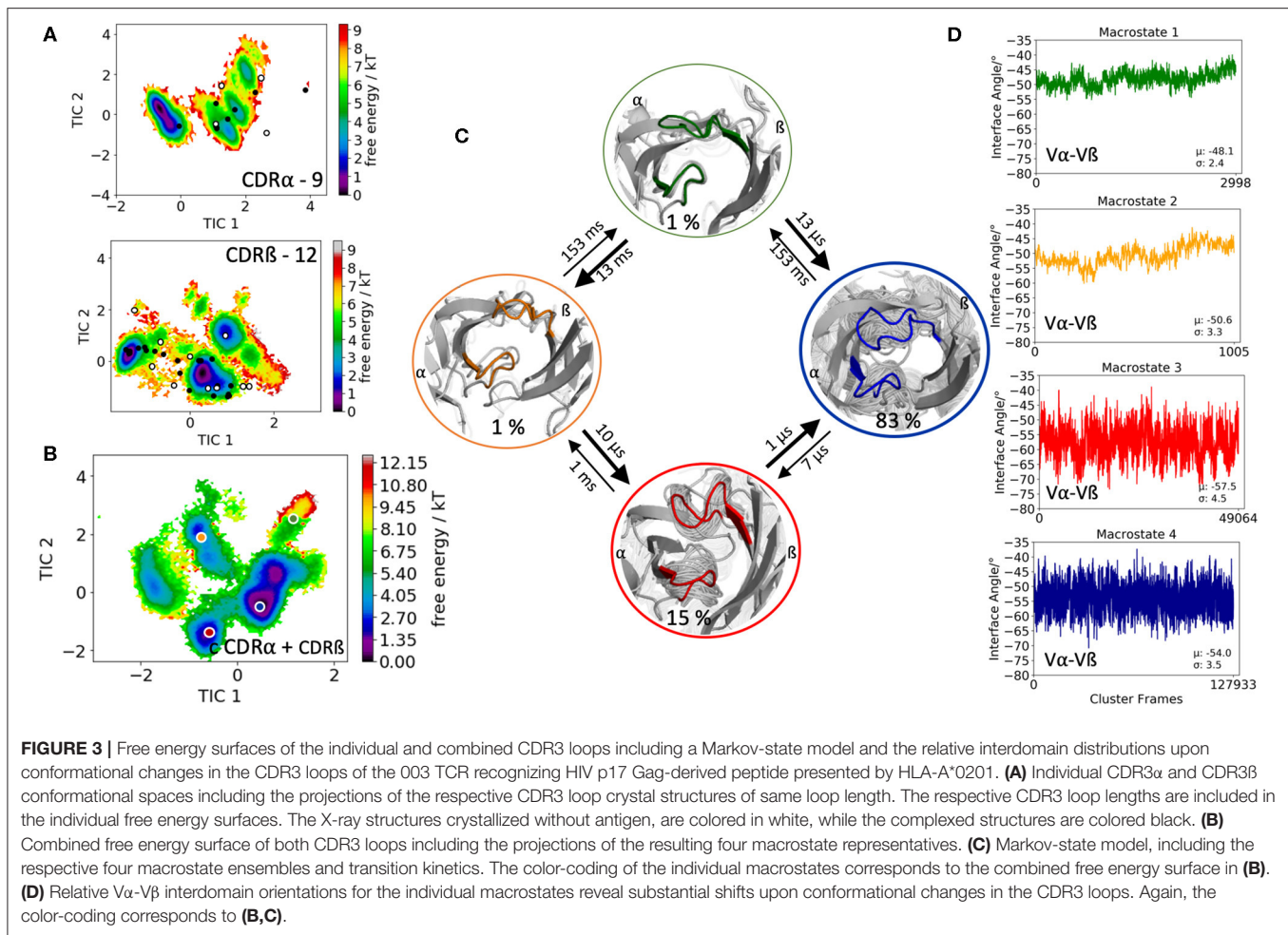


timescales in the micro-to-millisecond timescale. The macrostate representatives of the combined CDR3 loop tICA space are used to investigate the influence of different CDR3 loops on the relative interdomain distributions. **Figure 3D** illustrates the interface angle distributions of the respective macrostate ensembles and we observe a strong influence of the CDR3 loop states on the relative interface angle distributions.

The fourth TCR investigated, is the human melanoma specific TCR (E8) complexed with the MHC molecule and an epitope variant of the triosephosphate isomerase. E8 revealed very low affinity for the mutant triosephosphate isomerase-HLA-DR1, even though, the E8 cells have highly tumor-reactive properties (55). Three X-ray structures of the E8-TCR crystallized with and without antigen were available (PDB accession codes: 2IAM, 2IAN, 2IAL). As starting structure, we used the E8-TCR crystallized with antigen with the PDB accession code 2IAM. The biggest conformational differences upon antigen binding are located in the CDR3 loops. The CDR3 α loop length is 11, while the CDR3 β loop consists of 9 amino acids. The clustering of 1 μ s of metadynamics simulation resulted in 93 clusters and the obtained 9.3 μ s of trajectories were used to reconstruct thermodynamics and kinetics of the CDR3 loop conformational rearrangements in solution. Again, the individual

CDR3 α and CDR3 β loop conformational spaces are illustrated in **Figure 4A** and we observe that again the majority of available TCR crystal structures are present in solution. The combined free energy surface of the CDR3 ensembles is illustrated in **Figure 4B**. The Markov-state model in **Figure 4C** resulted in four macrostates with transition kinetics in the nano-to-microsecond timescales. We further used the macrostate ensembles to calculate the relative interdomain orientations to identify shifts upon conformational changes in the CDR3 loops (**Figure 4D**). In this case, we only observe small shifts in the interdomain angle distributions for different CDR3 loop conformational states.

The last TCR studied, is the 42F3 TCR, which is derived from an alloreactive cytotoxic T lymphocyte clone that recognizes MHC class I molecule H2-L^d presenting peptide p3A1 (PDB accession code 3TJH). The 42F3 TCR is related to another p-H2-L^d reactive TCR, the 2C TCR, which both recognize the related epitope of 2-oxoglutarate dehydrogenase, QL9. The only differences between the two TCRs are the different CDR3 sequences to recognize QL9-H2-L^d (56). The CDR3 α loop contains 12 residues, while the CDR3 β loop consists of 11 amino acids. Clustering resulted in 230 cluster representatives, which were used as starting structures for each 100 ns of molecular dynamics simulations. The 23.0 μ s of trajectories were used to

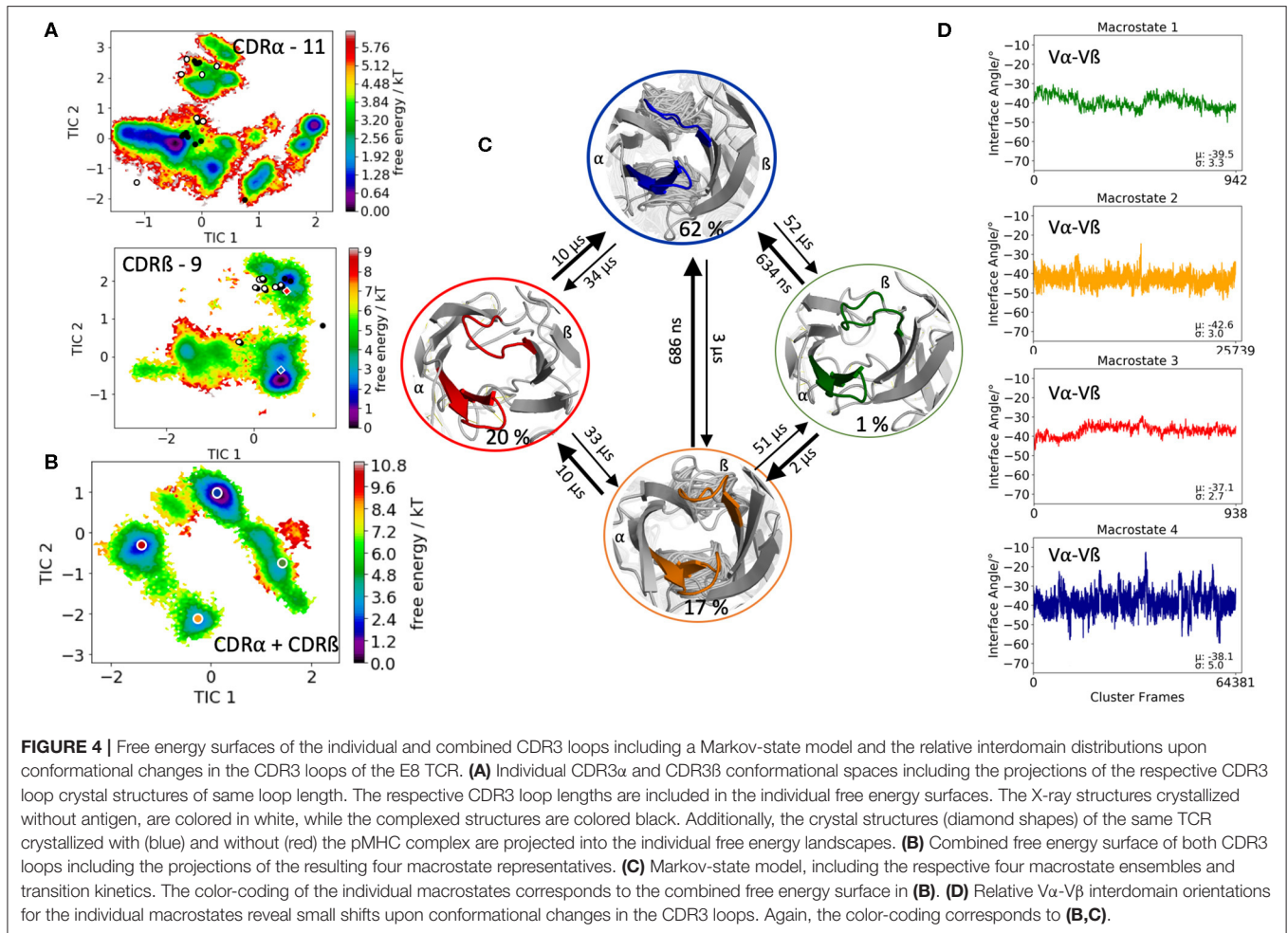


reconstruct kinetics and thermodynamics of the conformational rearrangements in the CDR3 loops and the influence of different CDR3 loop conformations on the relative V α -V β distributions. **Figure 5A** illustrates the free energy landscapes of the individual CDR3 α and CDR3 β loops including the projections of the available TCR CDR3 loop crystal structures of same length. Again, the majority of X-ray structures is present for the CDR3 α loop even another dominant minimum in solution could be identified, which is not apparent from X-ray maybe due to crystal packing effects. The combined free energy surface of the CDR3 loops and the respective Markov-state model are displayed in **Figures 5B,C**. We obtained four macrostates with kinetics in the low microsecond timescale. Additionally, we observe small shifts in the V α -V β distributions for different CDR3 loop macrostates upon conformational changes in the CDR3 loops. **Figure S9** shows a summary table of all observed V α -V β distributions with the respective averages and variances. To enhance the statistical significance of our results, we performed the Kolmogorov-Smirnov test to compare all macrostates of one TCR with each other (57). The respective *p*-values are illustrated in **Figure S10**. We clearly see that most of the distributions are different from each other and that conformational changes in the CDR3 loops, result in shifted interface angle distributions. Additionally, to

show the CDR loop flexibilities, especially of the CDR3 loops, we included in **Figure S11** the resulting RMSF plots of the respective macrostates.

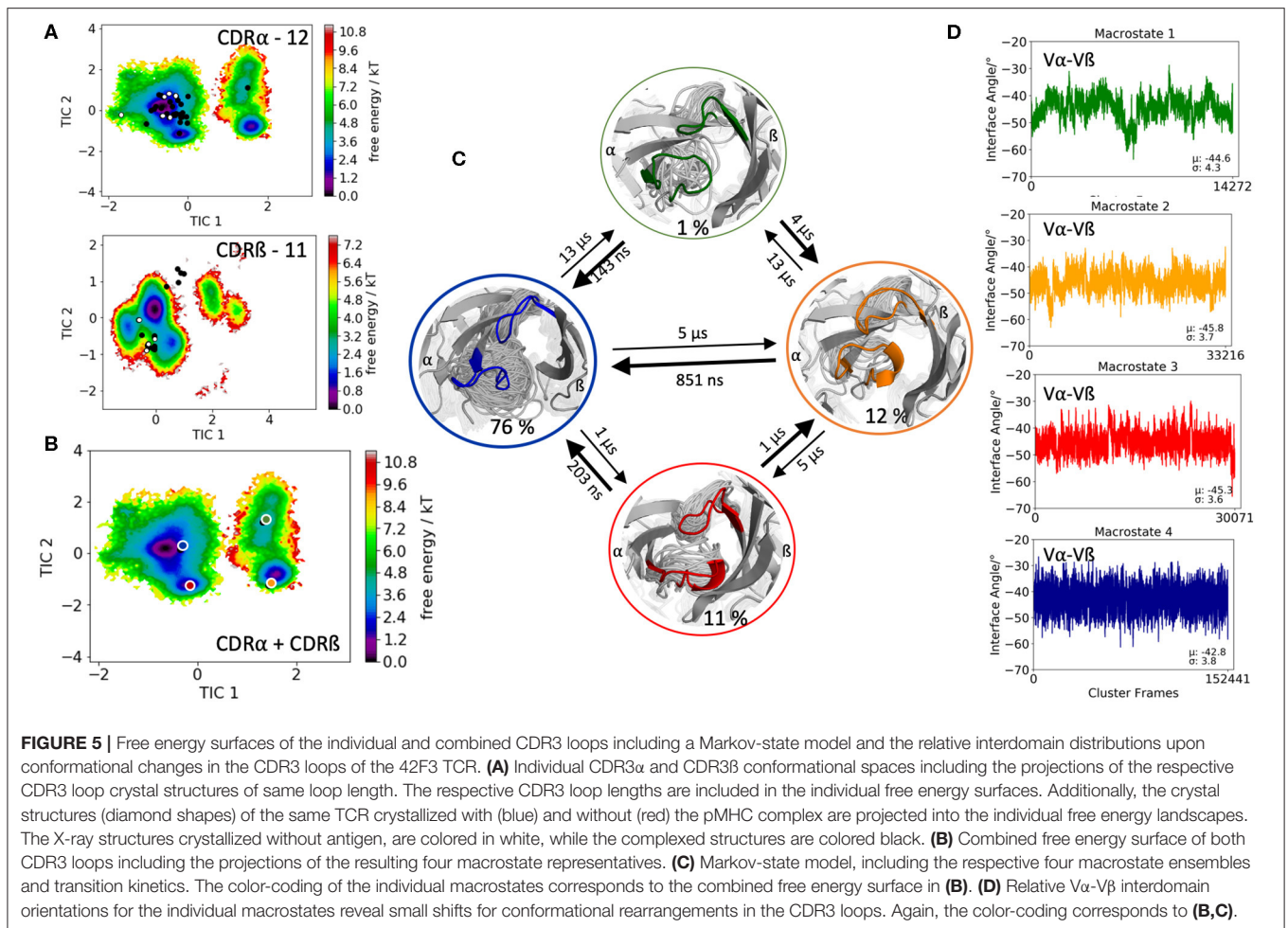
DISCUSSION

The outstanding flexibility and dynamics of TCR CDR loops has been the focus of various crystallographic and computational studies (16, 19). The same TCR was shown to adopt multiple loop conformations, indicating their crucial role in cross-reactivity (58). Additionally, a characterization of structure and dynamics of a TCR is essential to elucidate the antigen-binding mechanism, the involved conformational changes and the associated biological implications (4, 17, 18). X-ray studies comparing TCRs crystallized with and without the pMHC complex revealed a high flexibility in the binding interface (1, 3, 14, 17, 20). However, crystal structures represent only a snapshot of a specific protein conformation that can be distorted due to crystal packing effects (15, 59). Studies on antibodies and TCRs discussed the high flexibility of the CDR3 loops and the fact that a single static structure is not sufficient to capture the high conformational diversity of these loops (15, 16, 60–62). It has also been shown that the CDR3 α loop exhibits slower



and simpler movements, while the CDR3 β loop displays faster and more diverse loop rearrangements (16, 63). Characterizing the conformational diversity of TCR binding loops has been shown to play a crucial role in elucidating the antigen-binding mechanism and the TCR binding specificity (18, 64, 65). The concept of conformational selection suggests, that within this pre-existing ensemble of conformations, the binding competent state is selected, accompanied by a population shift of the conformational states (66–68). Depending on the probability of the conformation chosen by the binding partner, the binding mechanism is called “lock and key,” “conformational selection,” or “induced fit.” If the dominant apo state is selected as binding competent conformation, the binding is normally denoted as “lock and key” (69). If the binding selects an apo conformation that is observed before binding, i.e., this conformation has a high enough probability to be within the arbitrary detection limit of an experimental technique, the binding is called “conformational selection” (67, 68). Finally, if the binding occurs to a rare conformation, that is present before binding, but cannot be detected before binding—all conformations pre-exist, however, with varying probabilities—the process is interpreted as “induced fit” binding (Figure 7) (70).

This view on proteins that one sequence shows high conformational diversity and thus can adopt various conformations, facilitated the understanding of the evolution of new structures (71). A prime example for conformational selection is illustrated in Figure 1A. The B4.2.3 TCR binding to the pMHC ligand P18-I10 H2-D^d exhibits substantial structural differences upon binding in particular, in the CDR3 loops. Especially for the CDR3 β loop, we clearly see that even without the presence of the antigen the binding competent conformation lies in the dominant minimum in solution, while the X-ray structure crystallized without the antigen is situated in a local side minimum (Figure 1A). These observed structural changes in the CDR3 loops can be explained due to interactions of the TCR CDR3 loops with the tail region of the crystal symmetry mates (15, 72). Additionally, Figure 1A illustrates the high mobility and flexibility of the CDR3 loops and thereby provides insights into the immune recognition and selection mechanisms. The majority of available crystal structures are present within our obtained ensembles in solution. A possible assignment of the crystal structures to kinetic macrostates in solution is shown in Figure 6 for the CDR3 β loop. Various studies focused on characterizing the role of the CDR3 loops and identified strong



structural loop correlations in the peptide recognition process (13, 14, 19). As evidence for a structural correlation of the CDR3 loops has been provided, we reconstructed thermodynamics and kinetics for the combined CDR3 loops. The combined CDR3 conformational space in **Figure 1B** displays a shallow free energy surface with five macrostates. Excitingly, we were able to observe substantial shifts in the relative V α -V β distributions for conformational rearrangements in the CDR3 loops, indicating a strong dependency of the CDR3 loop conformations on the relative interface angle orientations. This strong influence of different CDR3 loop conformations can be explained because of their location in the center of the paratope and their major role in recognizing and binding to the peptide. In line with these results shifts in the relative V α -V β distributions can be observed for all studied TCRs (**Figures 2D, 3D, 4D, 5D**) highlighting the extraordinary conformational diversity and the correlation between the CDR3 loops and the interface angles. Previous studies have shown that the relative interdomain orientations reveal a high variability and fluctuate in the 0.1 GHz timescale. These results suggest that short molecular dynamics simulations are sufficient to capture the majority of accessible interdomain orientations (73). In agreement with these studies we observe that

the slow component of the relative V α -V β dynamics strongly correlates with conformational CDR3 loop rearrangements, which occur on the micro-to-millisecond timescale.

Another example of conformational selection is illustrated in **Figure 4A**. In line with the results in **Figure 1A**, even without the presence of the antigen the binding competent conformations of both the CDR3 α and CDR3 β are present and lie in the global minimum in solution, while the X-ray structure crystallized without antigen is distorted due to crystal packing effects and is located in a side minimum. **Figure S6** shows both the CDR3 α and CDR3 β conformational spaces, resulting of 14.4 μ s of trajectories, by using the X-ray structure, crystallized without antigen (PDB accession code 2IAL) as starting structure for molecular dynamics simulations. Also, in this example we observe, especially for the CDR3 α , in agreement with the results shown in **Figure 4A**, that the binding competent state is the dominant structure in solution, while the apo structure lies in a local shallow side minimum. **Figures S7, S8** show the observed crystal packing effects of the TCRs (**Figures 1, 4, respectively**) with their symmetry mate TCRs, highlighting the close contacts and interactions. These interactions and contacts result in different CDR3 loop conformations, which lie in

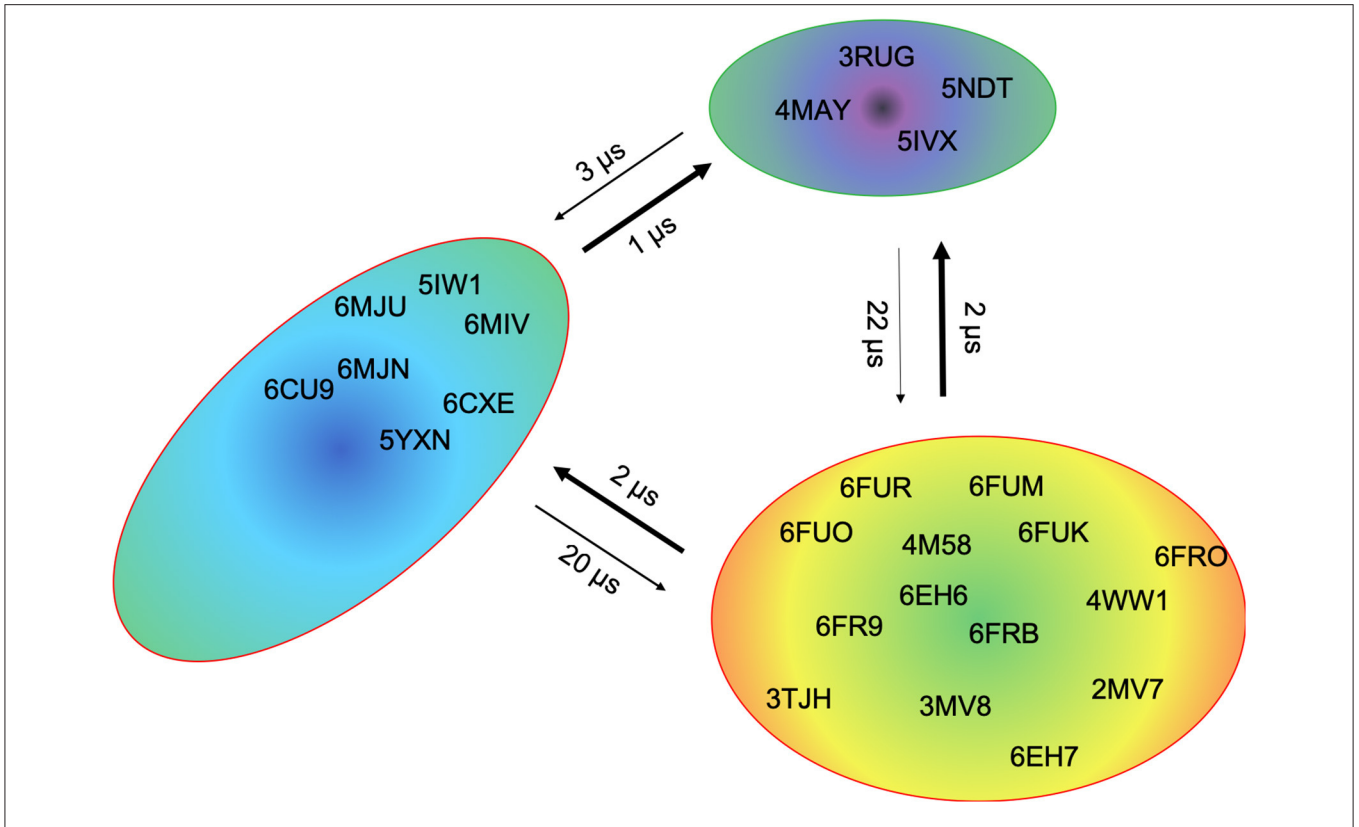


FIGURE 6 | Assignment of the available TCR crystal structures to kinetic macrostates for the B4.2.3 TCR CDR3 β loop with a loop length of 10 residues. The state probabilities correspond to the free energy surface in **Figure 1A** and are indicated in the color-coding. Additionally, transition timescales between the different macrostates in the low microsecond timescale can be observed.

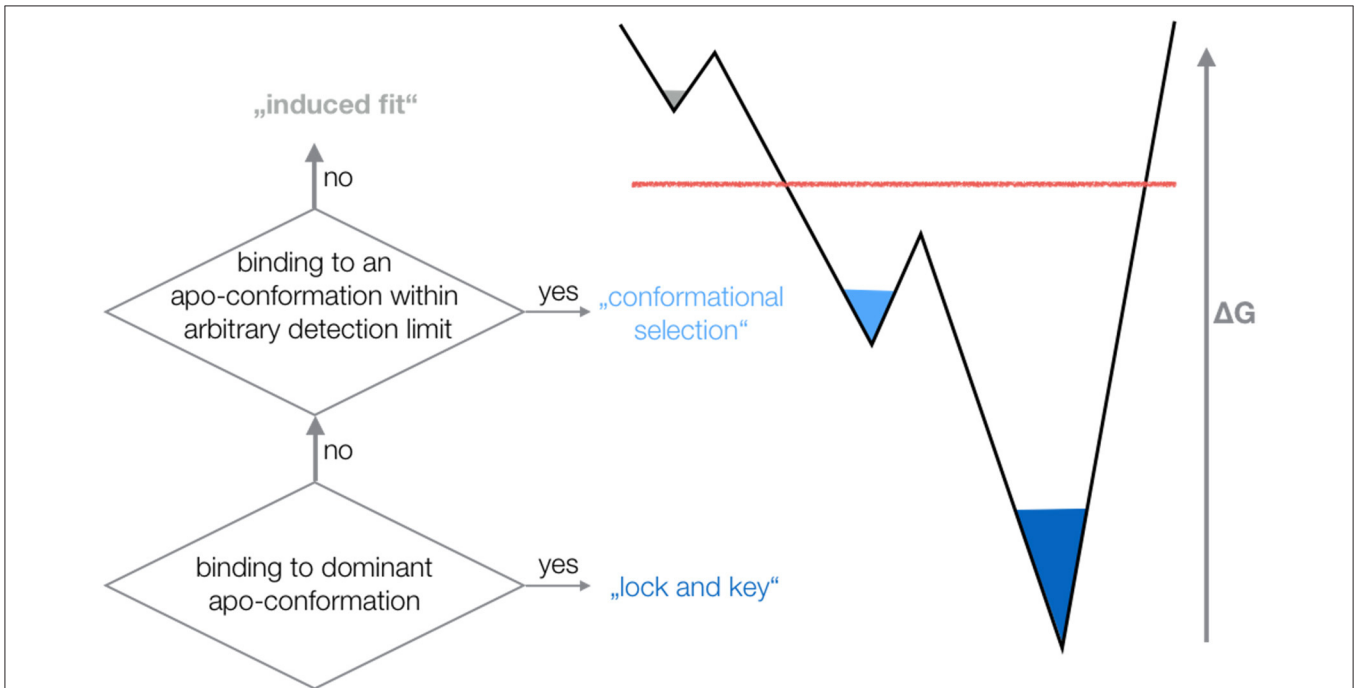


FIGURE 7 | Schematic illustration of different binding mechanisms and their relationship to conformational ensembles before binding. Depending on the probability of the conformation chosen by the binding partner, the binding mechanism is called “lock and key,” “conformational selection,” or “induced fit”.

local shallow side minima, while the complexed structures are present in the dominant minimum in solution. This distortion of CDR loops has already been observed and discussed in various examples for antibody Fabs, showing that antibodies are optimized to bind the antigen (15, 72). The fact, that the binding competent CDR3 loop conformations lie in the global minimum in solution, strengthened the confidence in our results. The 003 TCR recognizing HIV p17 Gag-derived peptide presented by HLA-A*0201 has already been studied to investigate the TCR loop flexibility and the influence of crystallization conditions on the resulting crystal structures. Our results are in perfect agreement with the observations of this study, that one single snapshot of a TCR is not enough to capture and understand this high conformational diversity. Especially the CDR3 β conformational space in **Figure 3B** illustrates the high flexibility of this crucial binding loop for peptide recognition, because not only the majority of available TCR crystal structures are present within the resulting ensemble in solution, but also another minimum could be identified, which is not apparent from X-ray structures, maybe due to crystal packing effects. Analogous to these observations, **Figure 2A** shows for both the CDR3 α and CDR3 β loops that besides capturing the majority of crystal structures, additional dominant solution structures have to be considered when characterizing CDR3 loops.

CONCLUSION

In this study we investigated five T-cell receptors with different CDR3 loop lengths and identified that the majority of available crystal structures of the same CDR3 loop lengths are present within the CDR3 loop ensembles in solution and some of them even belong to the same kinetic minimum. Thus, we observe that one TCR CDR3 loop can adopt various conformations and

thereby clearly follows the concept of conformational diversity. Additionally, these findings extend the model of static canonical clusters to a dynamic conformational ensemble. Thereby, to properly capture this high flexibility, the CDR3 loops need to be characterized as conformational ensembles. To identify the influence of the CDR3 loop conformational states on the relative V α -V β distributions we calculated a combined Markov-state model and the respective CDR3 macrostates in solution exhibited strong shifts in the relative interdomain V α -V β distributions for all studied TCRs upon changes in the CDR3 loop conformations.

DATA AVAILABILITY STATEMENT

All datasets presented in this study are included in the article/**Supplementary Material**.

AUTHOR CONTRIBUTIONS

The manuscript was discussed and written through contributions of all authors. All authors have given approval to the final version of the manuscript.

FUNDING

This work was supported by Austrian Science Fund (P30565 and P30737).

SUPPLEMENTARY MATERIAL

The Supplementary Material for this article can be found online at: <https://www.frontiersin.org/articles/10.3389/fimmu.2020.01440/full#supplementary-material>

REFERENCES

- Rudolph MG, Stanfield RL, Wilson IA. How TCRs bind MHCs, peptides, and coreceptors. *Annu Rev Immunol.* (2006) 24:419–66. doi: 10.1146/annurev.immunol.23.021704.115658
- van der Merwe PA, Dushek O. Mechanisms for T cell receptor triggering. *Nat Rev Immunol.* (2011) 11:47–55. doi: 10.1038/nri2887
- Wong WK, Leem J, Deane CM. Comparative analysis of the CDR loops of antigen receptors. *Front Immunol.* (2019) 10:2454. doi: 10.3389/fimmu.2019.02454
- Wilson IA, Christopher Garcia K. T-cell receptor structure and TCR complexes. *Curr Opin Struct Biol.* (1997) 7:839–48. doi: 10.1016/S0959-440X(97)80156-X
- Allison TJ, Winter CC, Fournié J-J, Bonneville M, Garboczi DN. Structure of a human $\gamma\delta$ T-cell antigen receptor. *Nature.* (2001) 411:820–4. doi: 10.1038/35081115
- Bentley GA, Boulout G, Mariuzza RA. The structure of the antigen-binding site of immunoglobulins and T-cell receptors. *Res Immunol.* (1995) 146:277–90. doi: 10.1016/0923-2494(96)80262-8
- Lawand M, Déchanet-Merville J, Dieu-Nosjean M-C. Key features of Gamma-Delta T-cell subsets in human diseases and their immunotherapeutic implications. *Front Immunol.* (2017) 8:761. doi: 10.3389/fimmu.2017.00761
- Chothia C, Lesk AM, Tramontano A, Levitt M, Smith-Gill SJ, Air G, et al. Conformations of immunoglobulin hypervariable regions. *Nature.* (1989) 342:877–83. doi: 10.1038/342877a0
- Al-Lazikani B, M Lesk A, Chothia C. Canonical structures for the hypervariable regions of T cell $\alpha\beta$ receptors. *J Mol Biol.* (2000) 295:979–95. doi: 10.1006/jmbi.1999.3358
- Hughes MM, Yassai M, Sedy JR, Wehrly TD, Huang C-Y, Kanagawa O, et al. T cell receptor CDR3 loop length repertoire is determined primarily by features of the V(D)J recombination reaction. *Eur J Immunol.* (2003) 33:1568–75. doi: 10.1002/eji.200323961
- Rock EP, Sibbald PR, Davis MM, Chien YH. CDR3 length in antigen-specific immune receptors. *J Exp Med.* (1994) 179:323–8. doi: 10.1084/jem.179.1.323
- Knapp B, van der Merwe PA, Dushek O, Deane CM. MHC binding affects the dynamics of different T-cell receptors in different ways. *PLoS Comput Biol.* (2019) 15:e1007338. doi: 10.1371/journal.pcbi.1007338
- Ayres CM, Scott DR, Corcelli SA, Baker BM. Differential utilization of binding loop flexibility in T cell receptor ligand selection and cross-reactivity. *Sci Rep.* (2016) 6:25070. doi: 10.1038/srep25070
- Yu K, Shi J, Lu D, Yang Q. Comparative analysis of CDR3 regions in paired human $\alpha\beta$ CD8 T cells. *FEBS Open Bio.* (2019) 9:1450–9. doi: 10.1002/2211-5463.12690
- Fernández-Quintero ML, Kraml J, Georges G, Liedl KR. CDR-H3 loop ensemble in solution – conformational selection upon antibody binding. *MAbs.* (2019) 11:1077–88. doi: 10.1080/19420862.2019.1618676
- Crooks JE, Boughter CT, Scott LR, Adams EJ. The hypervariable loops of free TCRs sample multiple distinct metastable conformations in solution. *Front Mol Biosci.* (2018) 5:95. doi: 10.3389/fmolb.2018.00095

17. Willcox BE, Gao GF, Wyer JR, Ladbury JE, Bell JI, Jakobsen BK, et al. TCR binding to peptide-MHC stabilizes a flexible recognition interface. *Immunity*. (1999) 10:357–65. doi: 10.1016/S1074-7613(00)80035-7
18. Hare BJ, Wyss DF, Osborne MS, Kern PS, Reinherz EL, Wagner G. Structure, specificity and CDR mobility of a class II restricted single-chain T-cell receptor. *Nat Struct Biol*. (1999) 6:574–81. doi: 10.1038/9359
19. Holland CJ, MacLachlan BJ, Bianchi V, Hesketh SJ, Morgan R, Vickery O, et al. *In silico* and structural analyses demonstrate that intrinsic protein motions guide T cell receptor complementarity determining region loop flexibility. *Front Immunol*. (2018) 9:674. doi: 10.3389/fimmu.2018.00674
20. Blevins SJ, Pierce BG, Singh NK, Riley TP, Wang Y, Spear TT, et al. How structural adaptability exists alongside HLA-A2 bias in the human $\alpha\beta$ TCR repertoire. *Proc Natl Acad Sci USA*. (2016) 113:E1276. doi: 10.1073/pnas.1522069113
21. Dubrovsky L, Dao T, Gejman RS, Brea EJ, Chang AY, Oh CY, et al. T cell receptor mimic antibodies for cancer therapy. *OncoImmunology*. (2016) 5:e1049803. doi: 10.1080/2162402X.2015.1049803
22. Trenevska I, Li D, Banham AH. Therapeutic antibodies against intracellular tumor antigens. *Front Immunol*. (2017) 8:1001. doi: 10.3389/fimmu.2017.01001
23. Dunbar J, Knapp B, Fuchs A, Shi J, Deane CM. Examining variable domain orientations in antigen receptors gives insight into TCR-like antibody design. *PLoS Comput Biol*. (2014) 10:e1003852. doi: 10.1371/journal.pcbi.1003852
24. Vargas-Madrado E, Paz-García E. An improved model of association for VH–VL immunoglobulin domains: asymmetries between VH and VL in the packing of some interface residues. *J Mol Recognit*. (2003) 16:113–20. doi: 10.1002/jmr.613
25. Bujotzek A, Lipsmeier F, Harris SF, Benz J, Kuglstatler A, Georges G. VH-VL orientation prediction for antibody humanization candidate selection: a case study. *MAbs*. (2016) 8:288–305. doi: 10.1080/19420862.2015.1117720
26. Labute P. Protonate3D: assignment of ionization states and hydrogen coordinates to macromolecular structures. *Proteins*. (2009) 75:187–205. doi: 10.1002/prot.22234
27. Molecular Operating Environment (MOE). Montreal, QC (2018).
28. Case DA, Betz RM, Cerutti DS, Cheatham TE III, Darden TA, Duke RE, et al. *AMBER 2016*. San Francisco, CA: University of California (2016).
29. Roe DR, Cheatham TE. PTRAJ and CPPTRAJ: software for processing and analysis of molecular dynamics trajectory data. *J Chem Theory Comput*. (2013) 9:3084–95. doi: 10.1021/ct400341p
30. Hub JS, de Groot BL, Grubmüller H, Groenhof G. Quantifying artifacts in Ewald simulations of inhomogeneous systems with a net charge. *J Chem Theory Comput*. (2014) 10:381–90. doi: 10.1021/ct400626b
31. Jorgensen WL, Chandrasekhar J, Madura JD, Impey RW, Klein ML. Comparison of simple potential functions for simulating liquid water. *J Chem Phys*. (1983) 79:926–35. doi: 10.1063/1.445869
32. Maier JA, Martinez C, Kasavajhala K, Wickstrom L, Hauser KE, Simmerling C. ff14SB: improving the accuracy of protein side chain and backbone parameters from ff99SB. *J Chem Theory Comput*. (2015) 11:3696–713. doi: 10.1021/acs.jctc.5b00255
33. Wallnoefer HG, Liedl KR, Fox T. A challenging system: free energy prediction for factor Xa. *J Comput Chem*. (2011) 32:1743–52. doi: 10.1002/jcc.21758
34. Barducci A, Bussi G, Parrinello M. Well-Tempered metadynamics: a smoothly converging and tunable free-energy method. *Phys Rev Lett*. (2008) 100:020603. doi: 10.1103/PhysRevLett.100.020603
35. Biswas M, Lickert B, Stock G. Metadynamics enhanced Markov modeling of protein dynamics. *J Phys Chem B*. (2018) 122:5508–14. doi: 10.1021/acs.jpcc.7b11800
36. Barducci A, Bonomi M, Parrinello M. Metadynamics. *WIREs Comput Mol Sci*. (2011) 1:826–43. doi: 10.1002/wcms.31
37. Abraham MJ, Murtola T, Schulz R, Páll S, Smith JC, Hess B, et al. GROMACS: high performance molecular simulations through multi-level parallelism from laptops to supercomputers. *SoftwareX*. (2015) 1–2:19–25. doi: 10.1016/j.softx.2015.06.001
38. Pronk S, Páll S, Schulz R, Larsson P, Bjelkmar P, Apostolov R, et al. GROMACS 4.5: a high-throughput and highly parallel open source molecular simulation toolkit. *Bioinformatics*. (2013) 29:845–54. doi: 10.1093/bioinformatics/btt055
39. Tribello GA, Bonomi M, Branduardi D, Camilloni C, Bussi G. PLUMED 2: new feathers for an old bird. *Comput Phys Commun*. (2014) 185:604–13. doi: 10.1016/j.cpc.2013.09.018
40. Ramachandran GN, Ramakrishnan C, Sasisekharan V. Stereochemistry of polypeptide chain configurations. *J Mol Biol*. (1963) 7:95–9. doi: 10.1016/S0022-2836(63)80023-6
41. Shao J, Tanner SW, Thompson N, Cheatham TE. Clustering molecular dynamics trajectories: 1. Characterizing the performance of different clustering algorithms. *J Chem Theory Comput*. (2007) 3:2312–34. doi: 10.1021/ct700119m
42. Case DA, Betz RM, Cerutti DS, Cheatham TE III, Darden TA, Duke RE, et al. *AMBER 2018*. San Francisco, CA: University of California (2018).
43. Salomon-Ferrer R, Götz AW, Poole D, Le Grand S, Walker RC. Routine microsecond molecular dynamics simulations with AMBER on GPUs. 2. Explicit solvent particle mesh Ewald. *J Chem Theory Comput*. (2013) 9:3878–88. doi: 10.1021/ct400314y
44. Miyamoto S, Kollman PA. Settle: an analytical version of the SHAKE and RATTLE algorithm for rigid water models. *J Comput Chem*. (1992) 13:952–62. doi: 10.1002/jcc.540130805
45. Berendsen HJC, Postma JPM, van Gunsteren WF, DiNola A, Haak JR. Molecular dynamics with coupling to an external bath. *J Chem Phys*. (1984) 81:3684–90. doi: 10.1063/1.448118
46. Adelman SA, Doll JD. Generalized Langevin equation approach for atom/solid-surface scattering: general formulation for classical scattering off harmonic solids. *J Chem Phys*. (1976) 64:2375–88. doi: 10.1063/1.432526
47. Scherer MK, Trendelkamp-Schroer B, Paul E, Pérez-Hernández G, Hoffmann M, Plattner N, et al. PyEMMA 2: a software package for estimation, validation, and analysis of Markov models. *J Chem Theory Comput*. (2015) 11:5525–42. doi: 10.1021/acs.jctc.5b00743
48. Chodera JD, Noé F. Markov state models of biomolecular conformational dynamics. *Curr Opin Struct Biol*. (2014) 25:135–44. doi: 10.1016/j.sbi.2014.04.002
49. Likas A, Vlassis N, Verbeek JJ. The global k-means clustering algorithm. *Pattern Recognit*. (2003) 36:451–61. doi: 10.1016/S0031-3203(02)00060-2
50. Röblitz S, Weber M. Fuzzy spectral clustering by PCCA+: application to Markov state models and data classification. *Adv Data Anal Classif*. (2013) 7:147–79. doi: 10.1007/s11634-013-0134-6
51. Karush J. On the Chapman-Kolmogorov equation. *Ann Math Statist*. (1961) 32:1333–7. doi: 10.1214/aoms/1177704871
52. Miroshin RN. Special solutions of the Chapman-Kolmogorov equation for multidimensional-state Markov processes with continuous time. *Vestnik St Petersburg Univ Math*. (2016) 49:122–9. doi: 10.3103/S1063454116020114
53. Wu H, Noé F. Variational approach for learning Markov processes from time series data. *J Nonlinear Sci*. (2017) 30:23–66. doi: 10.1007/s00332-019-09567-y
54. Keller AN, Eckle SBG, Xu W, Liu L, Hughes VA, Mak JYW, et al. Drugs and drug-like molecules can modulate the function of mucosal-associated invariant T cells. *Nat Immunol*. (2017) 18:402–11. doi: 10.1038/ni.3679
55. Deng L, Langley RJ, Brown PH, Xu G, Teng L, Wang Q, et al. Structural basis for the recognition of mutant self by a tumor-specific, MHC class II-restricted T cell receptor. *Nat Immunol*. (2007) 8:398–408. doi: 10.1038/ni1447
56. Adams JJ, Narayanan S, Liu B, Birnbaum ME, Kruse AC, Bowerman NA, et al. T cell receptor signaling is limited by docking geometry to peptide-major histocompatibility complex. *Immunity*. (2011) 35:681–93. doi: 10.1016/j.immuni.2011.09.013
57. Massey FJ. The Kolmogorov-Smirnov test for goodness of fit. *J Am Stat Assoc*. (1951) 46:68–78. doi: 10.1080/01621459.1951.10500769
58. Scott DR, Borbulevych OY, Piepenbrink KH, Corcelli SA, Baker BM. Disparate degrees of hypervariable loop flexibility control T-cell receptor cross-reactivity, specificity, and binding mechanism. *J Mol Biol*. (2011) 414:385–400. doi: 10.1016/j.jmb.2011.10.006
59. Rapp CS, Pollack RM. Crystal packing effects on protein loops. *Proteins*. (2005) 60:103–9. doi: 10.1002/prot.20492
60. Fernández-Quintero ML, Loeffler JR, Kraml J, Kahler U, Kamenik AS, Liedl KR. Characterizing the diversity of the CDR-H3 loop conformational ensembles in relationship to antibody binding properties. *Front Immunol*. (2019) 9:3065. doi: 10.3389/fimmu.2018.03065

61. Fernández-Quintero ML, Math BF, Loeffler JR, Liedl KR. Transitions of CDR-L3 loop canonical cluster conformations on the micro-to-Millisecond timescale. *Front Immunol.* (2019) 10:2652. doi: 10.3389/fimmu.2019.02652
62. Fernández-Quintero ML, Heiss MC, Pomarici ND, Math BA, Liedl KR. Antibody CDR loops as ensembles in solution vs canonical clusters from X-ray structures. *MAbs.* (2020) 12:1744328. doi: 10.1080/19420862.2020.1744328
63. Scott DR, Vardeman CF, Corcelli SA, Baker BM. Limitations of time-resolved fluorescence suggested by molecular simulations: assessing the dynamics of T cell receptor binding loops. *Biophys J.* (2012) 103:2532–40. doi: 10.1016/j.bpj.2012.10.037
64. Fernández-Quintero ML, Seidler CA, Liedl KR. T-cell receptor variable β domains rigidify during affinity maturation. *Sci Rep.* (2020) 10:4472. doi: 10.1038/s41598-020-61433-0
65. Glanville J, Huang H, Nau A, Hatton O, Wagar LE, Rubelt F, et al. Identifying specificity groups in the T cell receptor repertoire. *Nature.* (2017) 547:94–8. doi: 10.1038/nature22976
66. Boehr DD, Nussinov R, Wright PE. The role of dynamic conformational ensembles in biomolecular recognition. *Nat Chem Biol.* (2009) 5:789–96. doi: 10.1038/nchembio.232
67. Tsai C-J, Kumar S, Ma B, Nussinov R. Folding funnels, binding funnels, and protein function. *Protein Sci.* (1999) 8:1181–90. doi: 10.1110/ps.8.6.1181
68. Ma B, Kumar S, Tsai C-J, Nussinov R. Folding funnels and binding mechanisms. *Protein Eng Des Sel.* (1999) 12:713–20. doi: 10.1093/protein/12.9.713
69. Fischer E. Einfluss der configuration auf die Wirkung der enzyme. *Ber Dtsch Chem Ges.* (1894) 27:2985–93. doi: 10.1002/cber.18940270364
70. Koshland Daniel E. The key-lock theory and the induced fit theory. *Angew Chem Int Ed English.* (1995) 33:2375–8. doi: 10.1002/anie.199423751
71. James LC, Tawfik DS. Conformational diversity and protein evolution – a 60-year-old hypothesis revisited. *Trends Biochem Sci.* (2003) 28:361–8. doi: 10.1016/S0968-0004(03)00135-X
72. Fernández-Quintero ML, Heiss MC, Liedl KR. Antibody humanization—the influence of the antibody framework on the CDR-H3 loop ensemble in solution. *Protein Eng Design Select.* (2020) 32:411–22. doi: 10.1093/protein/gzaa004
73. Fernández-Quintero ML, Hoerschinger VJ, Lamp LM, Bujotzek A, Georges G, Liedl KR. VH-VL interdomain dynamics observed by computer simulations and NMR. *Proteins.* (2020) 88:830–9. doi: 10.1002/prot.25872

Conflict of Interest: The authors declare that the research was conducted in the absence of any commercial or financial relationships that could be construed as a potential conflict of interest.

Copyright © 2020 Fernández-Quintero, Pomarici, Loeffler, Seidler and Liedl. This is an open-access article distributed under the terms of the Creative Commons Attribution License (CC BY). The use, distribution or reproduction in other forums is permitted, provided the original author(s) and the copyright owner(s) are credited and that the original publication in this journal is cited, in accordance with accepted academic practice. No use, distribution or reproduction is permitted which does not comply with these terms.